research papers

A new method of creating minibeam patterns for synchrotron radiation therapy: a feasibility study

Yolanda Prezado,* Michel Renier and Alberto Bravin

ID17 Biomedical Beamline, European Synchrotron Radiation Facility, 6 Rue Jules Horowitz, BP 220, 38043 Grenoble Cedex, France. E-mail: prezado@esrf.fr

Several synchrotrons around the world are currently developing innovative radiotherapy techniques with the aim of palliating and possibly curing human brain tumors. Amongst them, microbeam radiation therapy (MRT) and, more recently, minibeam radiation therapy (MBRT) have shown promising results. In MBRT the beam thickness ranges from 500 to 700 μm with a separation between two adjacent minibeams of the same value, whilst in MRT the thickness is of the order of 25–50 μm with a distance between adjacent microbeams of the order of 200 μm. An original method has been developed and tested at the ESRF ID17 biomedical beamline to produce the minibeam patterns. It utilizes a specially developed high-energy white-beam chopper whose action is synchronized with the vertical motion of the target moving at constant speed. Each opening of the chopper generates a horizontal beam print. The method described here has the advantage of being simple and reliable, and it allows for an easy control of the patient safety in future clinical trials. To study the feasibility of the method, dosimetric measurements have been performed using Gafchromic HD-810 films and compared with Monte Carlo simulations. The results of this comparison are discussed.

Keywords: brain tumors; microbeam radiation therapy; minibeam radiation therapy; clinical trials; Monte Carlo simulations.

1. Introduction

Preclinical protocols using microbeam radiation therapy (MRT) have been carried out at the ESRF (Suortti & Thomlinson, 2003; Bravin, 2007) for more than 20 years after the first application made at the Brookhaven National Laboratory (Slatkin et al., 1995) with very promising results for the treatment of highly aggressive brain tumors.

MRT differs from other radiotherapy techniques since it uses an array of spatially fractionated X-ray beams (typically 25−50 μm wide and some hundreds of micrometres spaced); the ESRF biomedical beamline energy spectrum ranges from 50 to 500 keV with a mean energy of around 100 keV (Honkimäki & Suortti, 1992). The brain is irradiated by those high intense microbeams in one single exposure. The peak doses deposited in the tumor are higher than 300 Gy. Several experiments have shown the curing effect of MRT delivered to aggressive brain-tumor-bearing animals (Dilmanian et al., 2002, 2003; Laissue et al., 1998; Smilowitz et al., 2006; Slatkin et al., 1995), while it has been shown that those extremely high doses delivered in microbeams are well tolerated by healthy tissues (Miura et al., 2006; Laissue et al., 1999, 2001; Dilmanian et al., 2001). The sparing effect in the healthy tissues along the beam paths before and after the tumors in the different orientations has been attributed to rapid biological repair of the microscopic lesions by the minimally irradiated cells contiguous to the irradiated tissue slices. However, such high-intensity microbeams can only be produced by synchrotron sources and have other practical limitations for their clinical implementation. Following the principle of spatial fractionation, an extension of the MRT method has been proposed by Dilmanian et al. (2006): the so-called minibeam radiation therapy (MBRT). Recent studies have shown that beams as thick as 0.68 mm retain part of their sparing effect in the rats central nervous system. Brains of healthy rats have been irradiated with minibeams of thickness 0.68 mm and center-to-center distance of 1.36 mm. No observable paralysis or behavioral changes were found for deposited doses up to 170 Gy. In addition, they have shown that two such orthogonal microbeam arrays can be interlaced to produce a quasi-unsegmented field at the target, thus producing focal targeting (Dilmanian et al., 2006; Anschel et al., 2007). Their findings strongly support a potential application of interlaced minibeams to treat tumors with minimal damage to surrounding normal tissues, hence paving the way to MBRT to a new field of development. The advantages of using larger beams are as follows. (i) The possible use of higher-energy photons issued from specially tailored X-ray tubes without the need of a synchrotron source; at the same time, spatially fractionated beams would allow for keeping some of the tissue sparing

capabilities shown by smaller microbeams. (ii) The dose profiles of minibeams are not as vulnerable as those of microbeams to beam smearing from cardiosynchronous tissue pulsation (Poncelet *et al.*, 1992). It therefore became desirable to develop new techniques to generate minibeams with suitable dimensions and in a reliable way.

2. Materials and methods

2.1. Operation principle

The MRT facility recently upgraded at the ESRF (Renier *et al.*, 2008) offers the ideal conditions for such development. The beam dimensions at the target position may reach 41 × 4 mm (h × v), with a maximum dose rate presently in excess of 20000 Gy s^{-1} without filtering. A fast-acting white-beam shutter (Renier *et al.*, 2002) controls the irradiation start and end positions on the targets supported by a κ-geometry goniometer equipped with a fast vertical scanning device. This goniometer offers six axes of freedom for the accurate positioning of samples with a general precision better than 10 μm. It also allows the samples to be scanned vertically on a 150 mm total excursion. By combining the controlled vertical motion of the target with the action of a specially designed white-beam chopper, it becomes easy to generate horizontal minibeam prints on the target. The white-beam chopper is inspired by the design of another chopper with adjustable duty cycle previously built for imaging applications (Renier *et al.*, 2005). It consists of a series of ten tungsten carbide blades, each 6 mm thick, assembled in a squirrel cage shape (Fig. 1). Its axis of rotation is horizontal and it lies on the central axis of the horizontally extended X-ray beam. The edges of the tungsten carbide blades have been rounded by electro-erosion within a general mechanical tolerance of 10 μm. The chopper rotation is driven by a Danaher/Kollmorgen brushless motor model DBL3N00130 coupled to a Servostar 606 controller. The duty cycle of the white-beam chopper is precisely fixed at 50%. This implies that the time when the beam is on will be exactly equal to the time when the beam is off. The white beam passes through a white-beam shutter and is spatially fractionated by the white-beam chopper. The deposited dose is a function of the vertical target speed for a given value of the dose rate, and the minibeam size is a function of the chopper rotation speed (Fig. 2). The rotation speed of the chopper and the vertical speed of the target are therefore linked by the desired width and spacing of the minibeams. If, as in the example considered in this paper, we wish to generate 600 μm-wide minibeams separated by
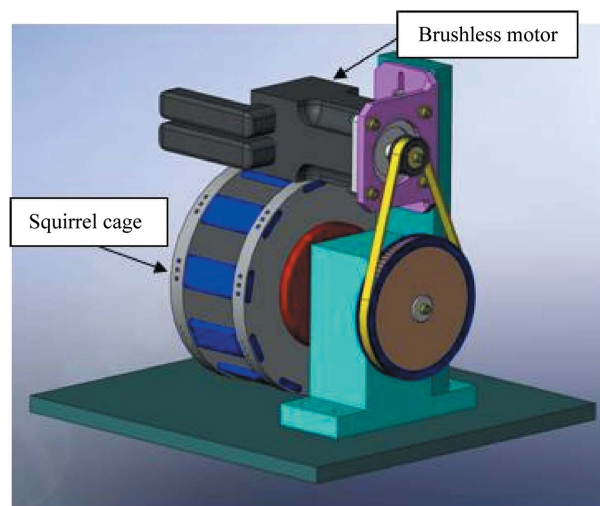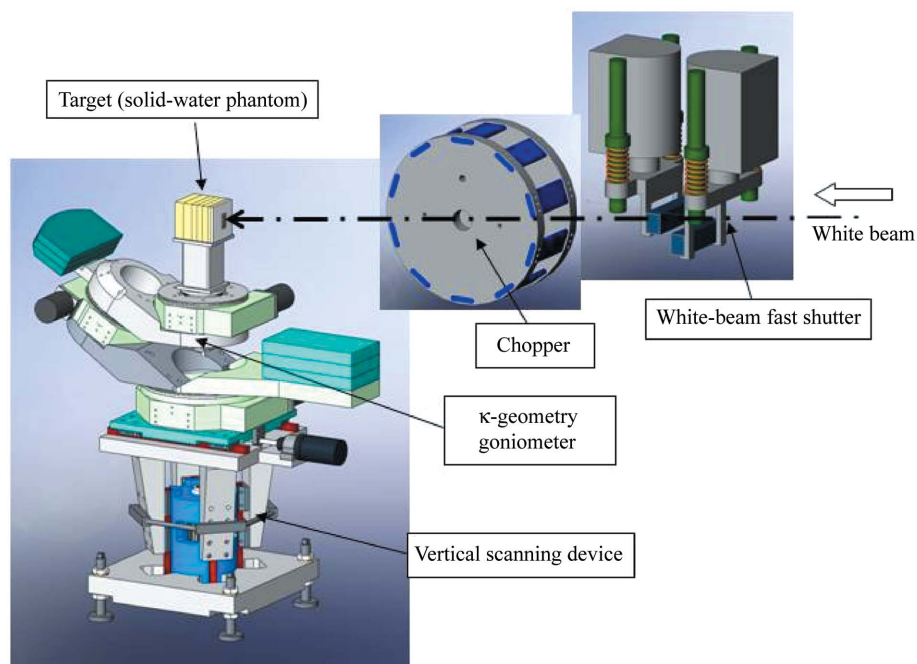

Figure 1
The white-beam chopper assembly.

600 μm, one complete revolution of the chopper must correspond to 10 × (0.6 + 0.6) mm, that is to say 1.2 mm of vertical displacement of the target, since the number of blades of the chopper is ten in its present construction.

In summary, a minibeam irradiation sequence includes seven steps.

(i) The available dose rate is accurately measured, under the operating conditions (storage-ring current, wiggler gap, metal filters inserted in the beam path, beam height).

(ii) The control software calculates and sets the chopper rotation speed and the target vertical speed for the desired

Figure 2
Experimental set-up. The white beam passes through a white-beam shutter and is later horizontally fractionated by the white-beam chopper. The rotation speed of the chopper is precisely synchronized with the vertical speed of the goniometer where the solid-water phantom is placed.

deposited dose, with some possible corrections if the storage-ring current has evolved.

(iii) The chopper rotation is triggered at the set value.

(iv) The vertical motion of the target is started following an acceleration ramp, and once the pre-defined irradiation area is reached.

(v) The white-beam fast shutter is opened, allowing the target minibeam irradiation, and then it is closed at the end of this area.

(vi) The vertical motion of the target is stopped after a deceleration ramp.

(vii) The rotary chopper rotation is stopped. The complete sequence is performed in a few tens of seconds.

2.2. Theoretical calculations: Monte Carlo simulations

In this work the percentage depth dose curves and transverse profiles of the dose deposited in a water phantom by the minibeams have been calculated by using Monte Carlo simulations. The *PENELOPE 2006* code has been used; *PENELOPE* is a general-purpose Monte Carlo simulation package developed at the University of Barcelona (Salvat *et al.*, 2003). The developers of this code have put special emphasis on the implementation of accurate low-energy electron cross sections, which are of particular importance for this application. Ten ideal minibeams of width 600 µm and center-to-center distance 1200 µm have been simulated. Neither the geometry of the blades of the chopper nor the beam divergence have not been included in the calculations. In all of the simulations the number of primary showers was 10^9.

2.3. Experimental conditions

The experiments were performed at beamline ID17 with closed wiggler gap (24.8 mm), in the 16-bunches mode, and with 75 mA current in the storage ring. The beam dimensions were limited to 25 mm horizontally and to 200 µm vertically by the beamline primary slits. In the beam path before the target the following filters were inserted: C (1.42 mm), Al (1.52 mm) and Cu (2.28 mm). Under these conditions the dose rate measured by an ionization chamber (PTW 31002) reaches 5350 Gy s^{-1}. As has already been explained in §2.1, one complete revolution of the chopper defines ten horizontal, equally spaced, minibeams on the target moving vertically at constant speed. For a beam thickness of 600 µm, one complete revolution of the chopper corresponds exactly to a vertical displacement of 12 mm for the target. As it has already been underlined, the deposited entrance dose is directly related to the vertical speed of the target and the rotation speed of the chopper. The goal was to reach 90 Gy at 8 cm depth in the solid-water phantom. Percentage depth dose curves obtained by Monte Carlo calculations were used in order to assess that the entrance peak dose needed to deliver 90 Gy at 8 cm was 300 Gy. In order to deposit this entrance dose in the phantom the vertical speed of the target was set at 12 mm s^{-1}, and the rotation speed of the chopper was then adjusted to 60 r.p.m. The preliminary performance results presented in this paper were obtained using a Gammex 457 solid-water phantom

Table 1
Peak-to-valley dose ratios (PVDR) at different depths obtained from Monte Carlo simulations (theoretical) and experimentally by using Gafchromic films; a good agreement is found.

| Depth (cm)	PVDR (theoretical)	PVDR (experimental)
2	11.3 ± 0.7	10 ± 2
4	9.6 ± 0.6	10 ± 2
8	8.9 ± 0.5	9.3 ± 1.5
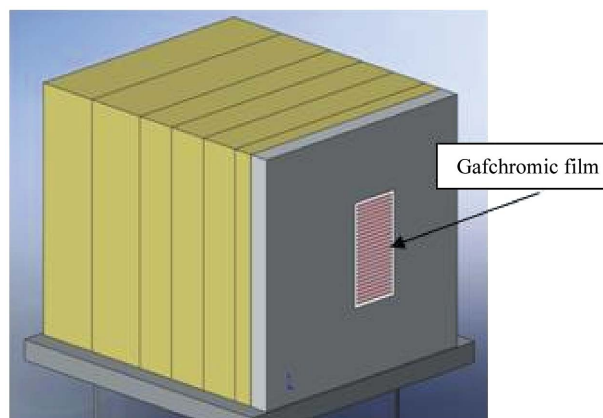
Figure 3
The solid-water phantom. It consists of a set of slices, among which some Gafchromic films are inserted.

offering the possibility of inserting Gafchromic HD-810 films at different depths from the surface (Fig. 3). The Gafchromic films were placed at 2, 4 and 8 cm depth from the entrance surface. They were irradiated with one complete revolution of the chopper. The Gafchromic films were read with a digital scanner (Epson Perfection V750 Pro) that had a resolution of 4800 dpi (approximately 5 µm). The dose profiles in the Gafchromic films were analyzed and compared with Monte Carlo simulations.

3. Results

The dose profiles analyzed at 2, 4 and 8 cm depth in the solid-water phantom were studied and compared with those obtained from Monte Carlo simulations. Table 1 shows a
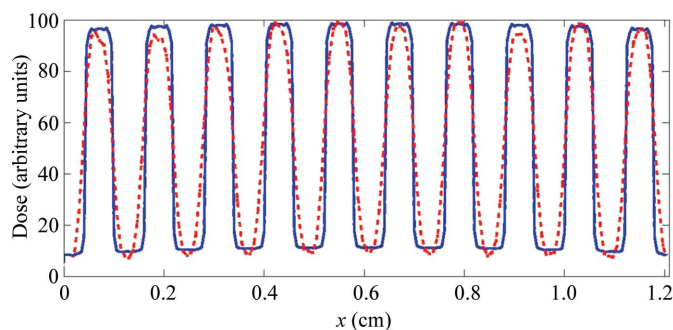
Figure 4
Comparison of the experimental dose profiles (red dashed line) and theoretical ones (blue solid line) at 8 cm depth in a solid-water phantom.

Table 2
Beam flatness at different depths obtained from Monte Carlo simulations (theoretical) and experimentally by using Gafchromic films.

Depth (cm)	Flatness (theoretical)	Flatness (experimental)
2	93 ± 1%	92 ± 4%
4	93 ± 1%	89 ± 4%
8	91 ± 1%	85 ± 5%

comparison of the peak-to-valley dose ratio (PVDR) values obtained from Monte Carlo simulations (theoretical) and those measured with the Gafchromic films. A good agreement is found between the experimental results and the theoretical calculations. Fig. 4 shows a comparison of the experimental and simulated dose profiles at 8 cm depth. The fact that valley doses are around the lower limit of the useful range of the HD-810 Gafchromic films (10–400 Gy) (International Specialty Products, http://online1.ispcorp.com/) is one cause of uncertainty on the PVDR determination. The PVDR decreases with depth as expected owing to the increase in the scattering filling the valley regions (Siegbahn *et al.*, 2006).

To characterize the dose profiles, three parameters (*i.e.* width, flatness and penumbras) have been studied and the results are discussed hereafter.

(i) The experimental full width at half-maximum (FWHM) was found to be 630 ± 50 μm, with no variation observed with depth within the error bars. The theoretical value is 600 μm, in agreement with the experimental data.

(ii) The flatness is specified as a maximum permissible percentage variation from the average dose across the central 80% of the FWHM of the profile in a plane transverse to the beam axis (Nath *et al.*, 1994). Table 2 shows a comparison of the experimental and theoretical values and here a good agreement is also found.

(iii) The penumbra is defined as the lateral distance between the 80% and 20% of maximum dose points on one side of a beam profile (Nath *et al.*, 1994). The experimental value obtained is 200 ± 30 μm, with no variation with depth within the error bars. The differences with the theoretical value from the simulations, 40 ± 5 μm, are due to the fact that the effects of the chopper blades and the divergence of the beam are not included in the Monte Carlo calculations.

In future work, further improvements of the flatness and penumbra of the profiles are expected by designing an appropriate flattening filter (Canaganayam *et al.*, 1995). The dosimetric analysis presented here shows the feasibility of the method. The results confirm that the vertical motion of the target was precisely synchronized with the action of the new chopper and that the chopper is able to produce minibeams whose dosimetric characteristics are similar to the ideal ones (simulations).

4. Conclusions

We have demonstrated that the proposed method is capable of accurately producing minibeam prints of high X-rays energies ($\gg 100$ keV). With the present geometrical dimensions of the squirrel cage, the duty cycle is fixed at 50%. The height of the minibeams is therefore exactly equal to their spacing and can easily be modified to optimize the efficiency of the MBRT, following the results of the preclinical trials in progress. The dosimetric analysis performed showed a good agreement with simulations. The experimental PVDR values, FWHM and beam flatness for different depths in a solid-water phantom agree with the calculations within the error bars. The experimental penumbras are larger than the theoretical ones, owing to the fact that neither the blades of the chopper nor the beam divergence have been modeled. The method offers an excellent reliability and allows for an easy control of all the parameters which are essential for the general safety of the treatment. The next step of this study will be to accurately position the first minibeam print on the target, in order to allow for the interlacing of a second and identical pattern of minibeams delivered from another orientation after rotation of the target around its vertical axis (Dilmanian *et al.*, 2006). This can be easily achieved by software control thanks to the absolute encoder available on the κ-geometry goniometer supporting the target, and to the precise control of the chopper brushless servo-motor. The perfect synchronization will be controlled by a hardware system comprising a perforated disc driven by the chopper and to guarantee the safe interlaced irradiation. The success of this feasibility study opens the door to biological studies on the curing capability of MBRT. If proven successful, this technique could conceivably be implemented in the future with high-power X-rays tubes.

References

Anschel, D. J., Romanelli, P., Benveniste, H., Foerster, B., Kalef-Ezra, J., Zhong, Z. & Dilmanian, F. A. (2007). *Minim. Invas. Neurosurg.* **50**, 43–46.

Bravin, A. (2007). *NATO Security Through Science Series B; Physics and Biophysics*, edited by V. Tsakanov and H. Wiedemann, pp. 225–239. The Netherlands: Springer.

Canaganayam, S., Hsu, W., Ferguson, S., Howlett, S., Denham, J. & Kron, T. (1995). *Australas. Phys. Eng. Sci. Med.* **18**, 53–56.

Dilmanian, F., Button, T., Le Duc, G., Zhong, N., Pena, L., Smith, J., Martinez, S., Bacarian, T., Tammam, J., Ren, B., Farmer, P., Kalef-Ezra, J., Micca, P., Nawrocky, M., Niederer, J., Recksiek, F., Fuchs, A. & Rosen, E. (2002). *Neuro-oncology*, **4**, 26–38.

Dilmanian, F., Morris, G., Le Duc, G., Huang, X., Ren, B., Bacarian, T., Allen, J., Kalef-Ezra, J., Orion, I., Rosen, E., Sandhu, T., Sathe, P., Wu, X., Zhong, Z. & Shivaprasad, H. (2001). *Cell Mol. Biol.* **47**, 485–493.

Dilmanian, F. A., Morris, G. M., Zhong, N., Bacarian, T., Hainfeld, J. F., Kalef-Ezra, J., Brewington, L. J., Tammam, J. & Rosen, E. M. (2003). *Radiat. Res.* **159**, 632–641.

Dilmanian, F. A., Zhong, Z., Bacariana, T., Benvenistea, H., Romanellia, P., Wangh, R., Welwarta, J., Yuasaa, T., Rosenj, E. M. & Anschela, D. J. (2006). *Proc. Natl. Acad. Sci. USA*, **103**, 9709–9714.

Honkimäki, V. & Suortti, P. (1992). *J. Appl. Cryst.* **25**, 97–104.

Laissue, J. A. *et al.* (2001). *Proc. SPIE*, **4508**, 65–73.

Laissue, J. A., Geiser, G., Spanne, P. O., Dilmanian, F. A., Gebbers, J. O., Geiser, M., Wu, X. Y., Makar, M. S., Micca, P. L., Nawrocky,

M. M., Joel, D. D. & Slatkin, D. N. (1998). *Int. J. Cancer*, **78**, 654–660.

Laissue, J. A., Lyubimova, N., Wagner, H. P., Archer, W., Slatkin, D. N., Di Michiel, M., Nemoz, C., Renier, M., Bräuer, E., Spanne, P. O., Gebbers, J. O., Dixon, K. & Blattmann, H. (1999). *Proc. SPIE*, **3770**, 38–45.

Miura, M., Blattmann, H., Bräuer-Krisch, E., Bravin, A., Hanson, A. L., Nawrocky, M. M., Micca, P. L., Slatkin, D. N. & Laissue, J. A. (2006). *Br. J. Radiol.* **79**, 71–75.

Nath, R., Biggs, P. J., Frank, J., Bova, C., Ling, C., Purdy, J. A., Van de Geijn, J. & Weinhous, M. S. (1994). *Med. Phys.* **21**, 1093–1121.

Poncelet, B. P., Wedeen, V. J., Weisskoff, R. M. & Cohen, M. S. (1992). *Radiology*, **185**, 645–651.

Renier, M., Brochard, T., Nemoz, C., Requardt, H., Bräuer, E., Estève, F., Balosso, J., Suortti, P., Baruchel, J., Elleaume, H., Berruyer, G., Berkvens, P. & Bravin, A. (2008). *Eur. J. Radiol.* **68**, S147–S150.

Renier, M., Brochard, T., Nemoz, C. & Thomlinsson, W. (2002). *Nucl. Instrum. Methods Phys. Res. A*, **479**, 656–660.

Renier, M., Fiedler, S., Nemoz, C., Gonzalez, H., Berruyer, G. & Bravin, A. (2005). *Nucl. Instrum. Methods Phys. Res. A*, **548**, 111–115.

Salvat, F., Fernández-Varea, J. M. & Sempau, J. (2003). *PENELOPE. A Code System for Monte Carlo Simulation of Electron and Photon Transport.* OECD Nuclear Energy Agency, Issy-les-Moulineaux, France. (Available in PDF format from http://www.nea.fr.)

Siegbahn, E. A., Stepanek, J., Bräuer-Krisch, E. & Bravin, A. (2006). *Med. Phys.* **33**, 3248–3259.

Slatkin, D., Spanne, P., Dilmanian, F., Gebbers, J. & Laissue, J. A. (1995). *Proc. Natl. Acad. Sci. USA*, **92**, 8783–8787.

Smilowitz, H. M., Blattmann, H., Bräuer-Krisch, E., Bravin, A., Di Michiel, M., Gebbers, J. O., Hanson, A. L., Lyubimova, N., Slatkin, D. N., Stepanek, J. & Laissue, J. A. (2006). *J. Neurooncol.* **78**, 135–143.

Suortti, P. & Thomlinson, W. (2003). *Phys. Med. Biol.* **48**, R1–R35.